Journal of Advanced Ceramics
2024, **13**(4): 403–412
https://doi.org/10.26599/JAC.2024.9220858

Research Article

Highly strengthening and toughening biomimetic ceramic structures fabricated via a novel coaxially printing

Kunkun Song[1,2,3], Shengda Yang[2,3], Ningqi Shao[2,3], Yantang Zhao[2,3], Peng He[2,3], Yongfeng Wei[2,3], Hengzhong Fan[1,✉], Yongsheng Zhang[1], Qiangqiang Zhang[2,3,✉]

[1] *State Key Laboratory of Solid Lubrication, Lanzhou Institute of Chemical Physics, Chinese Academy of Sciences, Lanzhou 730000, China*
[2] *School of Civil Engineering and Mechanics, Lanzhou University, Lanzhou 730000, China*
[3] *Key Laboratory of Mechanics on Disaster and Environment in Western China (Lanzhou University), Ministry of Education, Lanzhou 730000, China*

Received: November 28, 2023; Revised: December 28, 2023; Accepted: March 4, 2024

Abstract: Additive manufacturing technology, by manipulating and emulating inherent multiscale, multi-material, and multifunctional structures found in nature, has created new opportunities for constructing heterogeneous structures associated with special properties and achieving ultra-high mechanical performance and reliability in ceramic composite materials. In this study, we have developed an innovative fabrication method designated as coaxial 3D printing for the synchronous construction of two constituents into ceramic composites with a tooth enamel biomimetic microstructure. Herein, the stiff silicate and flexible epoxy served as a strengthening bridge and toughening layer, respectively. The method differed from the traditional approach of randomly dispersing reinforcing components within a ceramic matrix. It allowed for the direct creation of an internally effective three-dimensional reinforcement network structure in ceramic composites. This process facilitated synergistic deformation and simultaneous enhancement of multiple materials and hierarchical structures. Owing to the uniform distribution of internal stress and effective block of microcrack propagation, the biomimetically structured silicate/epoxy ceramic composite has demonstrated much significant enhancement in mechanical properties, including compressive strength (48.8±3.12 MPa), flexural strength (10.39±1.23 MPa), and flexural toughness (218.7±54.6 kJ/m³), which was 0.5, 2.1, and 47.5 times as high as those of the intrinsic brittle silicate ceramics, respectively. *In-situ* characterization and multiscale finite element simulation of microstructural evolution during three-point bending deformation further validated multiple-step features of the fracture process (silicate bridge fracture, interface detachment, epoxy extraction, and rupture), which benefited from interpenetrating structural features achieved by coaxial printing to accomplish with the complex propagating routines of the crack deflection in silicate ceramic composites. This coaxial 3D printing method paves the way for tailored toughening−strengthening designs for other brittle engineering ceramic materials.

Keywords: coaxial 3D printing; silicate ceramic composites; enamel biomimetic microstructure; strengthening bridge; toughening layer; crack deflection

1 Introduction

With the rapid development of modern science and technology and the growing demands of various industrial applications, humanity's specialized requirements for the structure and performance of engineering materials have become increasingly prominent [1,2]. Ceramic materials, in this context, represent a category of inorganic (non-metallic) materials prepared through the shaping process from natural or synthetically derived compounds. This category includes traditional silicate ceramics represented by high-temperature ceramics, cement, and glass, as well as specialized ceramics formed from oxides, carbides, and nitrides. Among these, engineering ceramic materials, particularly those based on silicates, stand out as fundamental materials extensively employed in major engineering structural components worldwide, garnering significant attention in fields such as aerospace and architectural engineering [3,4]. However, due to their intrinsic brittle features, highly disordered microstructure, and inevitable defects (e.g., weak interfaces, microcracks), traditional silicate ceramic composites generally fail to be employed in typical stress-yield structures [5,6]. Their unpredictable brittle damages are extremely prone to cause disastrous consequences when undergoing overloaded stress distribution, large deformations, natural disasters, and high-speed impacts [1,7]. The increased accumulation of cracks resulting from initiation and propagation processes over silicate ceramic composites greatly enhances probability of failure of structural components, which may pose a serious threat to human lives. The inevitable defects, strong chemical bonds, and weak grain boundaries in silicate ceramic composites jointly make them exclusive between the strength and the toughness for most engineering materials [8,9]. Therefore, conventional silicate ceramic composites must be reinforced by other ductile components prior to being considered for designs and

✉ Corresponding authors.
E-mail: H. Fan, hzhfan@licp.cas.cn;
Q. Zhang, zhangqq@lzu.edu.cn

清华大学出版社 Tsinghua University Press | SciOpen

implementations in engineering applications because of inherent brittleness [10,11].

Inspired by nature, biological structures, shaped through prolonged natural evolution, exhibit a very diverse array of mechanical structures with unique compositions and highly mechanical performance. Representative examples include highly mineralized nacre, moderately mineralized human bones and enamel, and low-mineralized tendons [12–14]. These biological materials, based on the ordered stacking of rigid and flexible phases across multiple hierarchical levels, possess mechanical strengthening characteristics that artificial materials with similar compositions cannot emulate. For instance, the tooth enamel with a parallel structure is composed of brittle enamel rods and flexible protein sheaths, which have been proved as one of the hardest tissues in the mammal body. Because of its orderly aligned interpenetration microstructure of the enamel, the mechanical properties (e.g., strength, modulus, and toughness) under compression deformation are much higher than those of engineered ceramics with similar constituents. Inspired by the enamel microstructure, the biomimetic ceramic composites with polymer polyvinyl alcohol serving as an elastic phase has demonstrated high fracture strength (1.6 GPa) and good elongation capacity (6.2%) [15–18]. For instance, the silicate-hydrogel biomimetic composites with a unidirectional and highly ordered microstructure realized a significant increase in flexural strength (4.73±0.34 MPa) and toughness (14,071±153 kJ/m^3) [19]. The structural biomimetic and flexible modification strategies have offered a combined effective pathway to synergistically enhance strength and toughness of engineering materials beyond the intrinsic brittle limitation of any individual constituent [20–24]. Nevertheless, the intricate structural architectures found in nature far exceed capabilities of traditional design and manufacturing technologies, impeding the progress of the structural material research and its applications in engineering systems. Additive manufacturing (3D printing), by manipulating and imitating inherent multiscale, multi-material, and multifunctional structures in nature, has created new opportunities for engineering design of complex material systems [2,14,25]. The early-reported biomimetic ceramic-based composite materials dated back to 1990 when Clegg *et al.* [26] employed a simple and cost-effective method to transform ceramic powders into sheets. They created a weak interface by coating the sheets with graphite, resulting in the composite materials with over four times higher fracture toughness compared to monolithic ceramics. Under comparable conditions, the required fracture energy was more than 100 times that of pure ceramics. To address the challenges of brittleness and susceptibility to cracking in ceramic structural materials, the concept of introducing weak interfaces was proposed. Subsequently, Wang *et al.* [27] successively proposed strategies for adjusting the composition and structure of soft/hard interfaces and enhancing the ceramic matrix layer to toughen ceramics. However, traditional blending methods face the limitations in the two-dimensional scale, including issues such as a blending threshold, easy aggregation, and uneven distribution. Simultaneously, the ceramic composites with high flexibility and weak interlayer interactions struggled to form micro/nano interfaces suitable for reinforcing, toughening, and strengthening large-scale and controllable assemblies. This greatly restricted the preparation of bulk ceramic-based composite materials [28,29].

Additive manufacturing (AM) has been demonstrated to be an effective approach for producing customized products with complex three-dimensional structures, applicable to various industries, including national defense, military, aerospace, and daily life. As a result, numerous novel additive manufacturing processes have been successfully developed [30,31]. This approach addresses the challenges of brittleness and complex structures quite effectively, but the issue of length proportions remains a concern, requiring further refinement. In particular, controlling interface properties and microstructure, identified as a "fatal weakness", proves challenging with the existing technology, thereby hindering its applications in engineering material structures [32,33]. Exploring how the strength of soft/hard interfaces can be controlled through smooth composition and mechanical gradients is of significant importance, aiming to reduce stress concentrations and delamination issues. This holds the key to overcoming the bottlenecks in 3D printing biomimetic ceramic materials.

In this article, the biomimetic silicate-epoxy composites with a tooth enamel-inspired microstructure was successfully fabricated via a novel coaxial 3D printing method. Drawing inspiration from the microstructure of teeth enamel, layers of silicate rods were deposited successively within the encapsulating epoxy resin sheath. Benefiting from this fabrication method, the stiff silicate-reinforced units and the flexible epoxy resin toughening layers formed an intricately interpenetrating microstructure after a sufficient mineralization reaction. Owing to the redistribution of internal stress, the suppression of the crack propagation, and the improvement of the interfacial slip, the 3D-printed biomimetic silicate-epoxy composite (BSEC) demonstrated highly improved mechanical properties including compressive strength (48.8±3.12 MPa), flexural strength (10.39±1.23 MPa), and flexural toughness (218.7±54.6 kJ/m^3) superior to traditional silicate-based composites. The microstructural evolution during the three-point bending deformation exhibited more complex routines of the crack prorogation in biomimetic structured silicate-based composites with much higher fracture energy consumption, validating the significant enhancement of flexural toughness. Therefore, the utilization of the coaxial printing method enables the synergistic construction of multiple components, paving the way for the innovative design and precise manufacturing of biomimetic brittle ceramic engineering materials accompanied by extraordinary mechanical properties.

2 Toughening mechanism of biomimetic enamel structure

2.1 Biomimetic enamel structure

Enamel, the outermost layer of teeth, plays a crucial role in achieving oral functionality and protecting underlying dentin and pulp cavity from mechanically induced damage. As the most mineralized biological tissue in mammals, it primarily consists of hydroxyapatite (HAP) mineral crystallites (96 wt%) and a small amount of protein mixture (4 wt%). Compared to other biological materials, the enamel exhibits a highly intricate multilevel layered structure with hierarchical complexities. It features high-brittleness fiber-like HAP crystallites robs, enveloped by flexible protein sheaths, all intricately bonded together as shown in Fig. 1(a). The toughening mechanism is illustrated in Fig. 1(b). When the compression-induced fracture causes cracks to traverse the biomimetic enamel structure, the bridging action of flexible sheath layers results in the crack deviation during the process of traversing multiple brittle rods. This diversion process of the crack propagation consumes more energy to move cracks forward, leading to toughening effects. The distinctive strong/weak

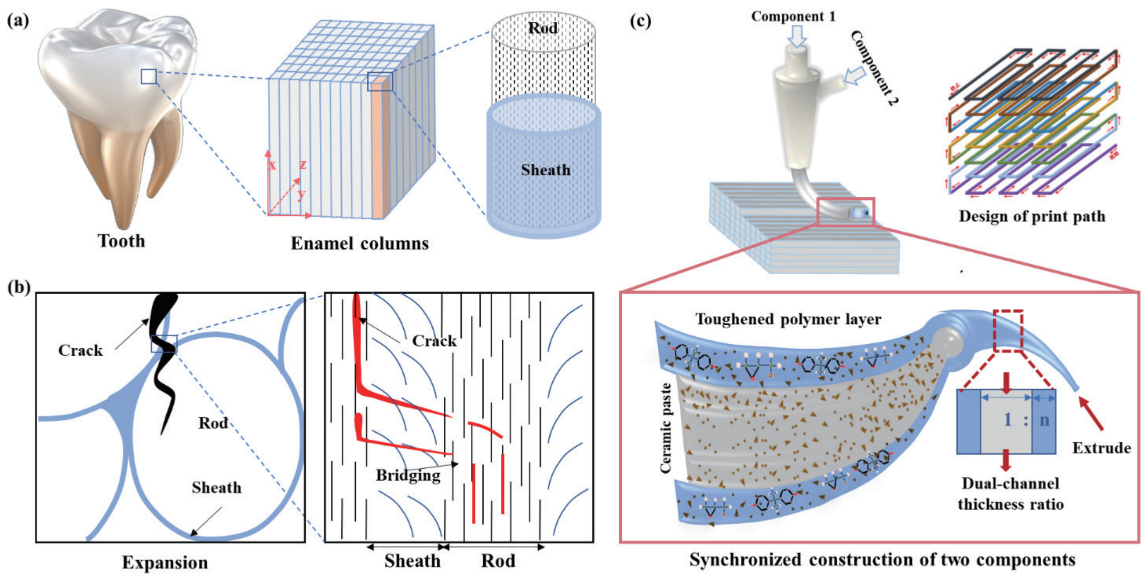

Fig. 1 Multilevel structure and toughening mechanism of tooth enamel and conceive of integrated construction: (a) internal structure of tooth enamel; (b) toughening mechanism of crack extension; (c) concept of dual-channel coaxial printing.

interface structure possesses unique properties surpassing any individual component, including high strength and fracture resistance. Therefore, the biomimetic structure of the enamel serves as one of the primary inspirations for toughening strategies in structural ceramic materials. As depicted in Fig. 1(c), inspired by the integrated structure construction of the tooth enamel, the initial concept of dual-component synchronous printing was proposed. By adjusting the thickness ratio of the dual channels and designing the printing path, a coaxial printing method was employed to fabricate ceramic-based composite materials mimicking the microstructure of the enamel.

2.2 Finite element simulation of compression damage in biomimetic enamel structure

To further validate effectiveness of the biomimetic enamel structure on the improvement of stress distribution and fracture characteristics, the finite element method (FEM) was comparatively conducted as illustrated in Fig. 2. A biomimetic enamel structure was designed (Fig. 2(a)), featuring silicate ceramic rods as the fundamental unit columns, each enveloped in a polymer (epoxy resin) sheath. The rod width was established at a ratio of 10 : 1 compared to the sheath thickness. The stress distribution characteristics and compression failure modes under three loading directions were analyzed using Mises stress (MPa) and compression failure field (Fig. 2(b)).

The FEM simulation revealed that the introduction of a interconnected polymer network into the ceramic matrix could change fracture features of the biomimetic enamel structure in different directions. Comparatively, pure ceramics (PCs) presented an X-shaped crack pattern under shear stress-induced fracture propagation along the 45° section (Fig. 2(c)), while the biomimetic ceramics (BCs) demonstrated the flexural failure along the *x*-axis. Fundamentally, all ceramic columns were paralleled to the *x*-axis, which mostly carried the compressing load under the transverse constraining of a polymer network. Cracks propagated along the biomimetic enamel structure interface from the top to the bottom as the brittle ceramic columns and flexible polymer layers underwent collaborative buckling and destabilization under compression.

In contrast, there is a significant dislocation slip phenomenon appeared for the crack propagation, which crossed interlayers of polymer for the loading process along the *y*-axis direction. When the compression load was applied along the *z*-axis, the evolution features of macroscopic cracks and stress distributions coincidently demonstrated that the interpenetrated microstructure of polymer and ceramic network could effectively lower stress level and change the direction of microcrack extension (Fig. 2(d)). Owing to higher ductility of the flexible polymer layer, the load was easily transferred to detached ceramic columns after the fracture appeared at the two-phase interface. The biomimetic enamel structure possessed superior strength along the *x*-axis rather than the other two loading directions with most silicate columns disrupted. The damage features were coincident with the results in the compression stress, validating the effectiveness of the interpenetrated flexible polymer network in improving strength and ductility beyond intrinsic brittleness of pure ceramic materials.

3 Preparation of biomimetic enamel ceramic composites

3.1 Raw materials and methods

The commercially available silicate ceramic powders were purchased from Shandong Yangchun Cement Co., Ltd. (China), and their main components were SiO_2 and CaO as listed in Table 1 according to X-ray fluorescence determination. Epoxy resin (EP) and polycarboxylic acid admixture (CQJ-JSS) were obtained from Shanghai Chenqi Chemical Technology Co. PVA (100 mesh) and polycarboxylic acid admixture (CQJ-JSS) were purchased from Shanghai Chenqi Chemical Technology Co. Deionized water was produced in-house at our laboratory in Lanzhou (China).

The particle size distribution of a silicate ceramic paste was analyzed using a laser particle size analyzer (LT2200, Linkoptik Instruments Co., Ltd., China). We evaluated rheological properties of extruded components using an intelligent rheometer (MCR302e, Anton Paar GmbH, Austria), and the testing temperature remained at 25 ℃. Microscopic characterizations were performed using a field emission scanning electron microscope (FESEM; S4800, Hitachi, Japan) at a working voltage of 20 kV. Microscopic computed tomography (CT; GE Phoenix V

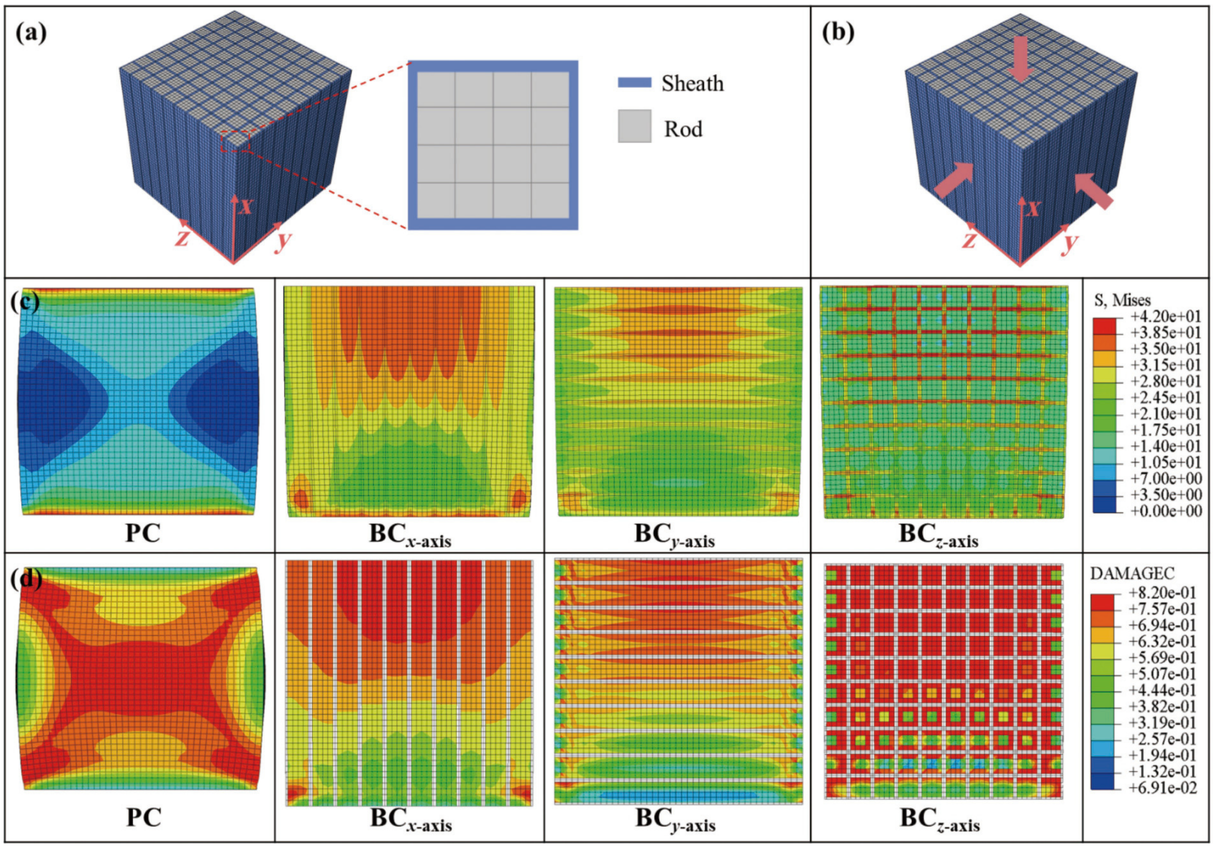

Fig. 2 FEM on damaging and stress-distributing features under compression: (a, b) design of micro-unit biomimetic enamel structure; (c, d) Mises stress and compression failure field.

Table 1 Chemical composition of silicates (Unit: %)

CaO	SiO_2	Fe_2O_3	Al_2O_3	K_2O	MgO	Na_2O	SO_3	Loss on ignition
44.09	20.85	3.01	9.08	0.95	3.36	0.71	2.47	3.15

tome X, UK) was used for cross-sectional scanning analysis and 3D reconstruction (maximum resolution: 1 μm).

3.2 Coaxial printing platform and needle design

To precisely fabricate biomimetic ceramic structures with the desired inner diameter (2–4 mm), tube thickness (0.5–1 mm), and geometric features (such as circular and square shapes), various coaxial nozzles tailored for synergistic printing of multiple materials were specifically designed to optimize flow behavior of ceramic pastes within microchannels (Figs. 3(a)–3(d)). The coaxial printing platform was operated by the direct ink writing method, which enables to the creation of an interpenetrated structure with two components (brittle and flexible) extruded cooperatively. Thereinto, the internal channel was filled with the ceramic paste, while the external channel delivered the second flexible phase of polymer (Fig. 3(e)). The cross section of the dual-channel nozzle and the flow behavior of slurry are illustrated in Fig. 3(f).

Based on numerical calculations of the continuous flow of two inks, we employed a coaxial printing needle with an inner diameter of 1.8 mm and a square geometric feature for coaxial extrusion. This needle was manufactured using stereolithography. The method allows for the creation of an intertwined structure formed by extruding silicates and EP together. In this setup, the internal channels were filled with the silicate paste, while the external channels were filled with freshly mixed EP gel. By adjusting geometric dimensions of coaxial nozzles with different inner and outer diameters, we varied the thickness ratio between the square silicate rod (1.8 mm × 1.8 mm) and the EP sheath (n = 0.05, 0.10, 0.25, and 0.50). The silicate paste suitable for printing was a mixture of silicate ceramic powders, deionized water, polyvinyl alcohol, and carboxylate salts in a weight ratio of 1 : 0.32 : 0.035 : 0.001. Subsequently, a precise layer-by-layer coaxial printing method was used to create dental enamel-like biomimetic silicate–EP composite materials with an intertwined microstructure. The EP gel was extruded at a flow rate of 4 mm/s, with layer thicknesses of 0.09, 0.18, 0.45, and 0.90 mm, while the silicate paste core materials (side length: 1.8 mm) were co-printed at the same speed.

3.3 Rheological properties of pastes

Fundamentally, the rheological and the isotropic properties of the printing paste dictate printability, significantly impacting the construction of 3D printed structures, structural stability, and geometric accuracy. The properly controlled shear stress is a crucial factor in maintaining the geometric shape of ceramic structures. As depicted in Fig. 4(a), with an increase in the shear stress, the printed sample's shape initially improves, but later deteriorates. Too low shear stress corresponds to low modulus and high fluidity of the paste, leading to severe plastic deformation and susceptibility to collapse under self-weight. On the other

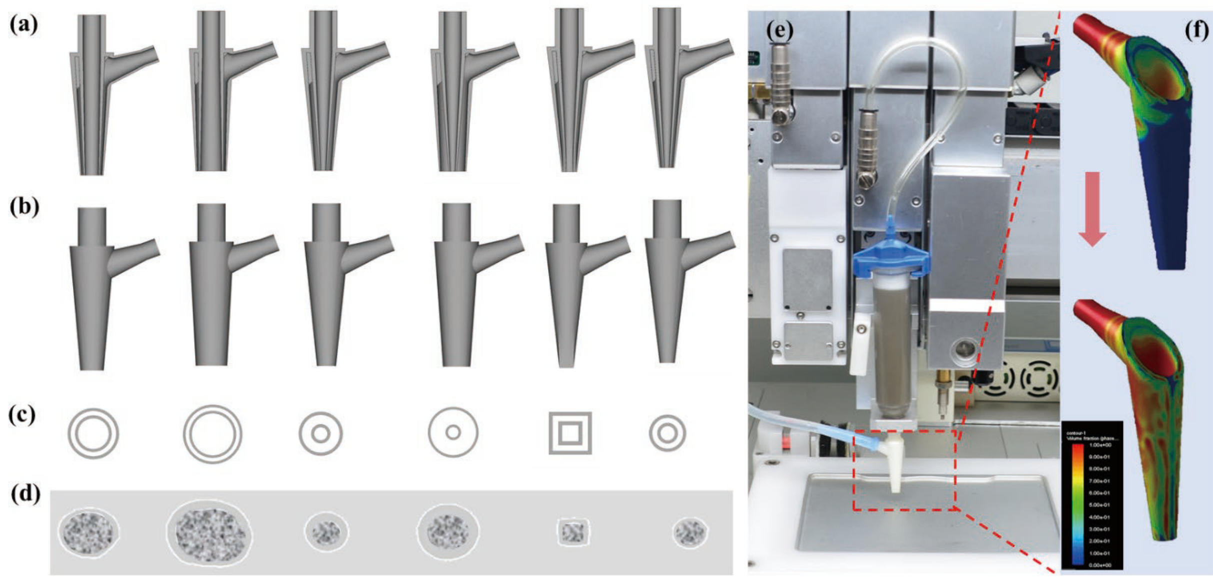

Fig. 3 Topological design of coaxial needles and printing platform. (a–c) Internal structure, external morphology, and nozzle shape of coaxial needles, respectively. (d) Morphologies of paste extruded through coaxial needles. (e) Schematic diagram of coaxial printing. (f) Flow behavior of slurry in nozzle.

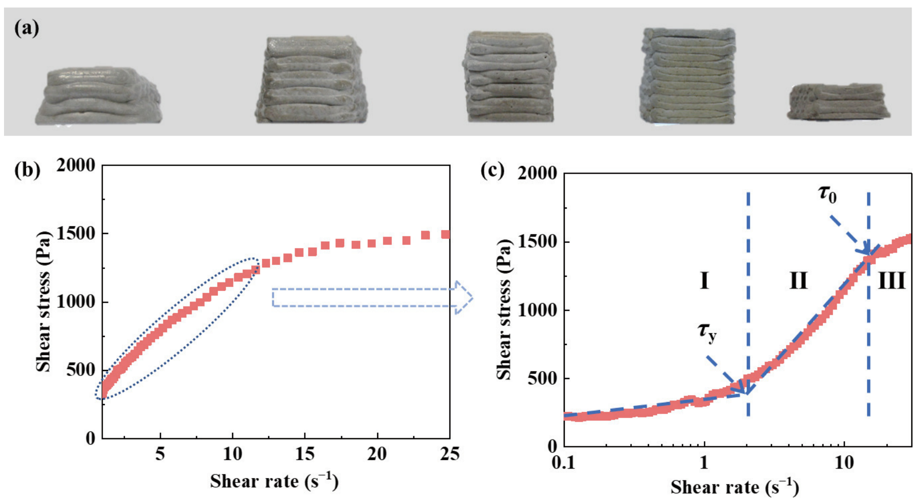

Fig. 4 Controlled fabrication for coaxially printing: (a) optical images of printed samples as shear stress increases; (b, c) rheological state analysis of silicate ceramic paste.

hand, excessive shear stress results in weak bonding at the material-printing interface, poor continuity, and an increased number of defects caused by slight plastic deformation. Specific analysis revealed, as illustrated in Figs. 4(b) and 4(c), that the silicate ceramic pastes exhibited distinct pseudo-plastic behavior and interfacial slip characteristics at low shear rates. When shear stress surpasses the yield shear stress (τ_y), the paste exhibits Newtonian fluid behavior (stage II). The shear stress increases linearly with the shear rate, which is presented as typical of Bingham model as shown in Eq. (1):

$$\tau = \tau_y + K\dot{\gamma} \tag{1}$$

where τ is the shear stress (Pa), $\dot{\gamma}$ is the shear rate (s^{-1}), K is the consistency coefficient (Pa·s), and τ_y is the yield stress.

As shear stress continues to rise, the paste demonstrated shear thinning behavior (stage III), with the shear stress dependent on the shear rate as Herschel–Bulkley model (Eq. (2)) [34]. This revealed a shear thinning effect as expected for a printable silicate ceramic paste, ensuring the print-on-demand within a hollow needle over the critical yield stress (τ_0) as defined in Eq. (2):

$$\tau = \tau_0 + K\dot{\gamma}^m \tag{2}$$

where m is the non-Newtonian index.

3.4 Microstructure characterization of biomimetic enamel

As shown in Fig. 5(a), a silicate-epoxy biomimetic sample was created by the coaxial 3D printing method of the silicate paste and epoxy resin gel, which exhibited a typically perpendicular array that was inspired by the tooth enamel. Along the three planes of *z–y*, *x–y*, and *z–x*, the micro-CT images of the silicate-epoxy sample exhibited a highly ordered alignment of printed silicate rods formed via layer-by-layer deposition (Figs. 5(b)–5(d)). Both stiff silicate rods and epoxy flexible layer were coherently interlocked to obtain a robust microstructure with interpenetrating features. Under the three-axis constraints of an interconnected epoxy resin framework, a tooth enamel biomimetic structure prepared by coaxial 3D printing enabled the significant improvement in mechanical strength and toughness beyond brittle silicate, which was always in a three-phase loading condition at microscale under the global compression along a

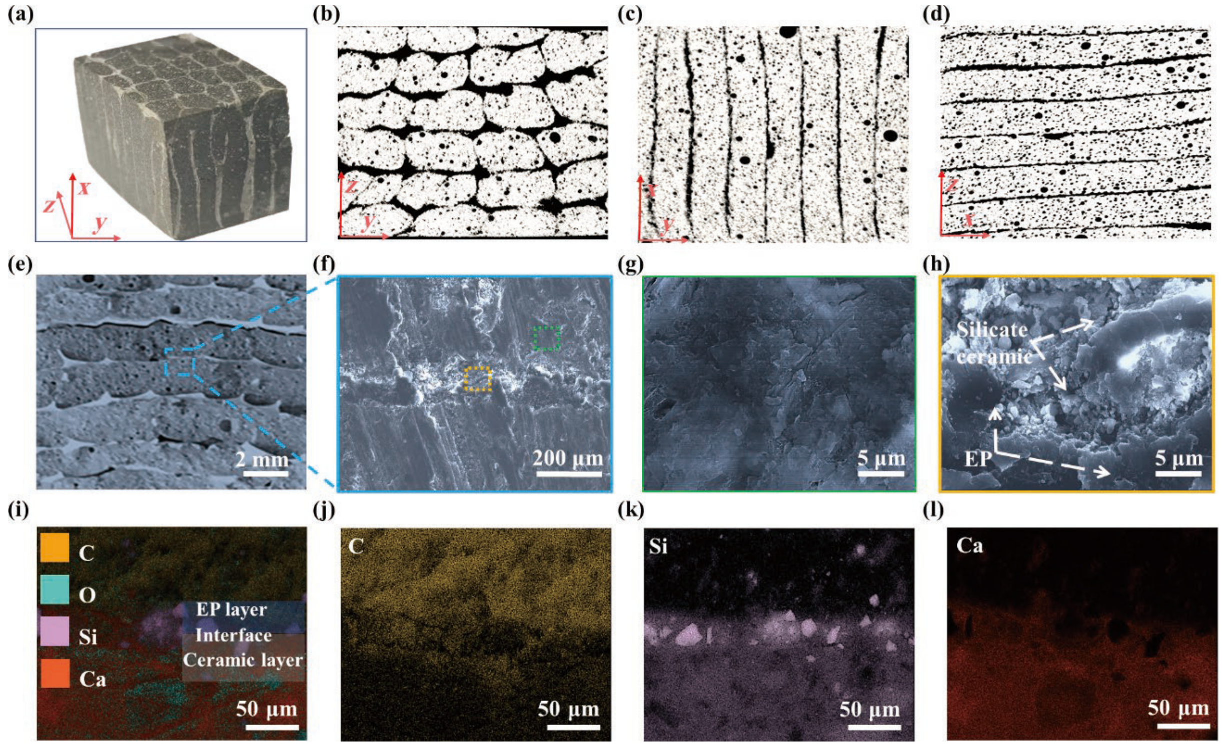

Fig. 5 Micro-macrostructural and elemental distribution characterizations of tooth enamel biomimetic silicate-epoxy ceramic composites: (a) optical photograph of printed sample; (b–d) micro-CT images along *z*–*y*, *x*–*y*, and *z*–*x* planes, respectively; (e–h) morphologies of silicates and silicate-epoxy interface. (i–l) EDS mappings of C, Si, and Ca around selected interface regions, respectively.

certain direction. The low-density region (black area) in the silicate cores consisted of EP-rich zones and pores, which generally increased in proportion to the EP content.

As depicted on the fracture surface (Fig. 5(e)), a certain degree of slip effect occurred at the interface between the mineralized products of the coaxially printed silicate ceramic pastes and the epoxy resin layers during fracture. Moreover, a seamless bonded interface was observed at the bonding location (Fig. 5(f)). The high-resolution SEM images, as shown in Figs. 5(g) and 5(h), further validated the mutual interpenetration microstructure of silicate ceramics and epoxy resin. This would facilitate the improvement of mechanical properties of coaxially printed silicate-epoxy biomimetic composites to overcome fatigue or corrosion impacts. The EDS mappings in Figs. 5(i)–5(l) for a selected region at the interface presented the uniformly distributed morphologies of chemical elements such as C, Si, and Ca, indicating that the flexible epoxy resin layer was stably embedded within the rigid silicate ceramic rods.

4 Mechanical properties of coaxial printed biomimetic silicate-epoxy ceramic composites

4.1 Impacts of dual-channel thickness ratio on compressive properties

To further verify the effect of the epoxy resin layer on mechanical strength and toughness, the thickness ratios (n) of the epoxy resin sheath to the silicate rods were adjusted from 0 to 0.5. As shown in Fig. 6(a), with n increased from 0.05 to 0.5, the compressive strength along the *x*-axis of the 3D printed biomimetic silicate-epoxy ceramic composites exhibited a decreased tendency from 51.2 to 26.2 MPa, while elongation capability increased from 3.1% to 3.7%. It was noteworthily noted that the maximum elastic strain reached up to 5.5% from the primary 2% for pure silicate ceramics. The compressive strength for $n \leq 0.25$ surpassed that of pure silicate ceramic materials when loading along the *x*-axis. The significant enhancement in compression strength and maximum elastic strain revealed the effectiveness of enamel biomimetic structural design methodology.

Similarly, the compressive strength along the *y*-axis demonstrated the primary rising but subsequently reducing tendency with the increase of epoxy layers' thickness in Fig. 6(b). The optimal thickness ratio was 0.05 with maximum compressive strength up to 38.8±3.12 MPa, which was higher than that of pure silicate ceramics (31.9±0.26 MPa) or other controllable cases. However, the compressive strength along the *z*-axis in Fig. 6(c) presented a comparable improvement in ductility but insufficient enhancement in strength depending on features. The reason for this difference was higher stacking density along the *y*-axis, a result of gravitational effects on the upper layers under printing constraints. This conclusion was corroborated in Fig. 5(b). In contrast, the 3D-printed biomimetic silicate-epoxy composites presented a more effective improvement on both strength and toughness along the *x*-axis than the other two directions the same as the tooth enamel biomimetic. The comparison of compressive performance among three directions (*x*, *y*, and *z*) revealed that the enamel biomimetic structure enables the most favorable improvement in mechanical properties along a specific direction (Fig. 6(d)).

4.2 Impacts of dual-channel thickness ratio on flexural properties

Furthermore, the three-point bending test was conducted to evaluate the improvement in flexural strength and toughness, which was perpendicular to the *x*-axis as shown in Fig. 7(a). The flexural strength of 3D-printed biomimetic silicate-epoxy ceramic composites presented a huge dependence on the epoxy layer's

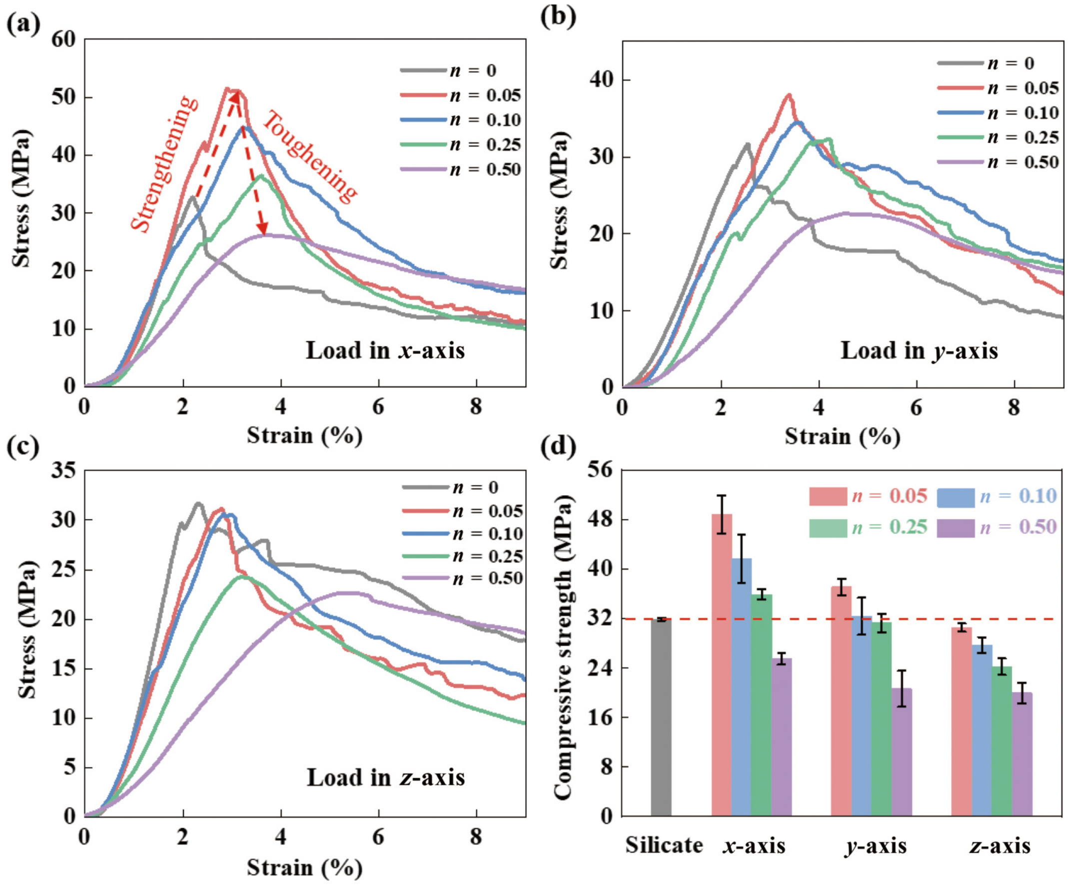

Fig. 6 Impacts of epoxy resin layer thickness on mechanical properties of 3D printed biomimetic silicate-epoxy composites: (a–c) uni-axial compression tests along *x*-, *y*-, and *z*-axis, respectively; (d) comparative strength under compressive deformation corresponding to three loading directions.

thickness. The maximum strength and elastic deflection reached up to 11.6 MPa and 0.86 mm corresponding to the thickness ratio (n) of 0.5. Noticeably, printed silicate-epoxy ceramic composites could hold substantial residual strength after silicates bridging cracks if n over 0.1 mm, significantly improving transient brittle fracture behavior for conventional silicate ceramic composites.

Compared with an intrinsically brittle silicate slab with an ultimate deflection of only about 0.06 mm, the tooth enamel biomimetic structure made 3D printed silicate-epoxy ceramic composites have much higher ductility and strength synchronously. The statistical maximum flexural strength (10.39±1.23 MPa) was over 2 times larger than that of the pure silicate paste (4.84±0.29 MPa), as well as over 13.8 times for elastic deformation capacities (Figs. 7(b) and 7(c)). Moreover, as shown in Fig. 7(d), the fracture energy of printed silicate-epoxy ceramic composites significantly enhanced with an increase in the epoxy layer thickness. The maximum fracture energy for n of 0.5 reached up to $(2.7\pm0.8)\times10^5$ N/m, which was over 50 times higher than that of the pure silicate paste ($(5.1\pm0.5)\times10^3$ N/m) (Fig. 7(d)). The related maximum flexural toughness (n = 0.5) increased from 4.6±1.7 kJ/m^3 for pure silicates to 218.7±54.6 kJ/m^3 for biomimetic ceramic composites (Fig. 7(e)).

Generally, traditional silicate-based ceramic composites are well-known for their high brittleness and low toughness. However, the 3D coaxial printing method created an enamel biomimetic structure featuring alternating flexible epoxy and stiff silicate phases. The printed silicate-epoxy ceramic composites demonstrated significant improvement in mechanical properties (e.g., strength, toughness) after optimizing the routines of crack propagation, which finally resulted in an effective increase of the flexural strength along a specific direction. According to the comparative results listed in Fig. 5(f), the biomimetic silicate-epoxy ceramic composites exhibited much higher toughness compared to those of reported silicate-based engineering materials, including pure silicate pastes, reinforced silicate composites, and engineering ceramics [43,44]. For instance, it was about 5 and 2 times as large as that of polymer fibers and steel fiber-reinforced silicate composites under the same density, respectively.

4.3 Damage feature under fracture deformation

As shown in Fig. 8, both finite element method (FEM) simulation and experimental observation cooperatively revealed that the introduction of the interconnected epoxy network into a silicate ceramic matrix could significantly alter fracture features of silicate-epoxy resin ceramic composites, further validating the effectiveness of coaxially printed biomimetic structure in improving stress distribution and fracture characteristics. In the model, the silicate ceramic part was designed with the size of 1.8 mm × 1.8 mm, while the external epoxy resin sheath was set as 0.18 mm in thickness to simulate the thickness ratio of 0.1 (Fig. 8(a)). The geometric model of a 3D printed silicate-epoxy beam consists of 5 × 5 matrixes with a span-to-height ratio of 1/4. The S33 stress field (tensile stress as positive and compressive stress as negative) provides comprehensive information on the principal stress state of the beam under z-axis conditions, aiding in identifying regions particularly prone to fracture. As shown in Figs. 8(b) and 8(c), when the pure silicate ceramic slab was subjected to a three-point bending deformation, the maximum tensile stress concentrated at the middle location of the span and

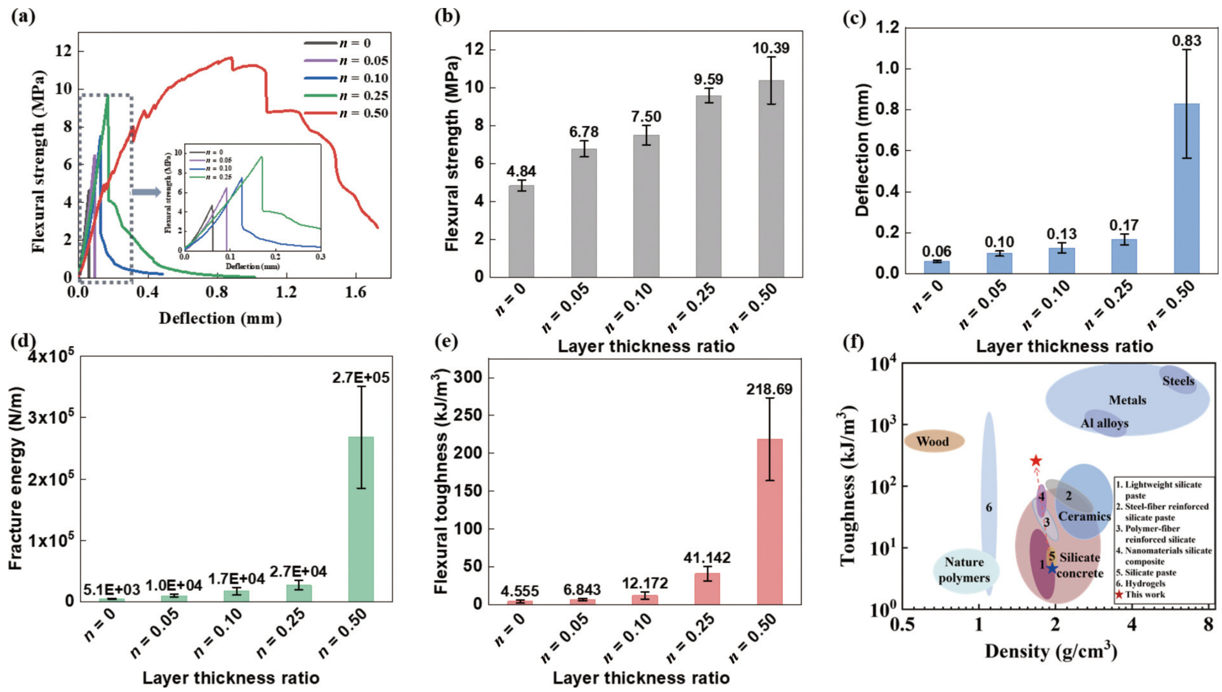

Fig. 7 Three-point bending performance of 3D printed silicate-epoxy biomimetic ceramic composites: (a) flexural strength depends on deflection; (b–e) comparative flexural strength, deflection, fracture energy, and flexural toughness, respectively; (f) toughness comparison with other materials [35–46].

oblique section at two edges, which led to unpredictable brittle damages under tensile and shear stress without ductile deformation, respectively.

In contrast, with the combination of an interpenetrated epoxy resin network, the re-distribution effect of internal stress optimized the strain of the silicate component. An arch-sharped stress mapping could effectively lower the stress concentration at the middle span. The epoxy layer enabled the rapid and straight propagation of cracks as long as the stress in the silicate part increased over the critical value. This mechanism made the crack change the direction to subsequently propagate along the interface of the silicate rod and epoxy layer. Until the epoxy layer was pulled out or fractured, the crack then extended to the next silicate rod. The epoxy layer failure was accompanied by micro-crack sprouting and interfacial sliding. This significantly improved the brittle feature of pure silicate composites. As a result, the complex routine for crack propagation made the coaxial printed biomimetic silicate-epoxy ceramic composites dissipate more fracture energy under larger permissible deformation and multiple deflecting interfaces, which realized the synergistic strengthening and toughening.

To qualitatively describe stress evolution, the related profiles along the different axes at critical locations were extracted, as shown in Fig. 8(d). The stress of the silicate slab gradually decreased due to its low ultimate tensile strength, which was prone to cause tensile damage. In contrast, the epoxy layer afforded much higher tensile stress within 3D-printed silicate-epoxy composites than that of the silicate part but with lower compressive strain. This facilitated the conversion of the fracture mode and further improvement in flexural strength and toughness. As depicted in Fig. 8(e), the stress profiles along the x-axis at different depths in the section A were created to distinguish the different stress levels on silicates and epoxy, respectively. For the depth = 0, the loading state was in compressing status with the epoxy resin layer displaying much lower stress. When the depth gradually increased (> 1/4), the internal stress gradually transferred to the tensile condition with the stress increased from 6.7 to 25.5 MPa under adjustment of the epoxy resin layer. Higher tensile stress in flexible epoxy resin generated a larger stress gradient, which could eliminate stress concentrations in the brittle silicate components. Such reinforcing mechanism primarily accounts for the significant improvement of toughness for biomimetic silicate-epoxy ceramic composites [19,47,48]. As a result, the stress in the section B was divided into two characteristic zones (zone I in tension and zone II in compression) as shown in Fig. 8(f). The stress profiles along the x-axis of the epoxy resin layer presented an arch-shaped distribution feature, while the tensile stress of the silicate component was uniformly retained at a lower level. The FEM simulation revealed that the involvement of the interpenetrated flexible phase (e.g., epoxy resin) within the silicate-based biomimetic structure prepared based on the coaxial 3D printing method can effectively improve the crack extension behavior of brittle silicate-based ceramic composites and cooperatively enhance flexural strength and toughness.

5 Conclusions

Advanced preparation methods or technologies are the trends of synergistically constructing complex heterogeneous structures and high-performance biomimetic composites. In this study, inspired by the high-strength and toughness natural structure of enamel's soft/hard interface, a novel coaxial printing method for the preparation of ceramic composites is developed. This method can achieve the simultaneous extrusion of two components by internally constructing a three-dimensional epoxy resin "sheath" network structure and a highly ordered silicate ceramic "rod". It successfully realizes an interpenetrating microstructure of two components (brittle silicate ceramics and flexible epoxy resin) and produces biomimetic enamel-like silicate-epoxy ceramic composites. The characterizations of SEM and micro-CT have validated results. Owing to synergic constraints of the silicate rod and epoxy resin interlayer at the microscale, the 3D coaxial

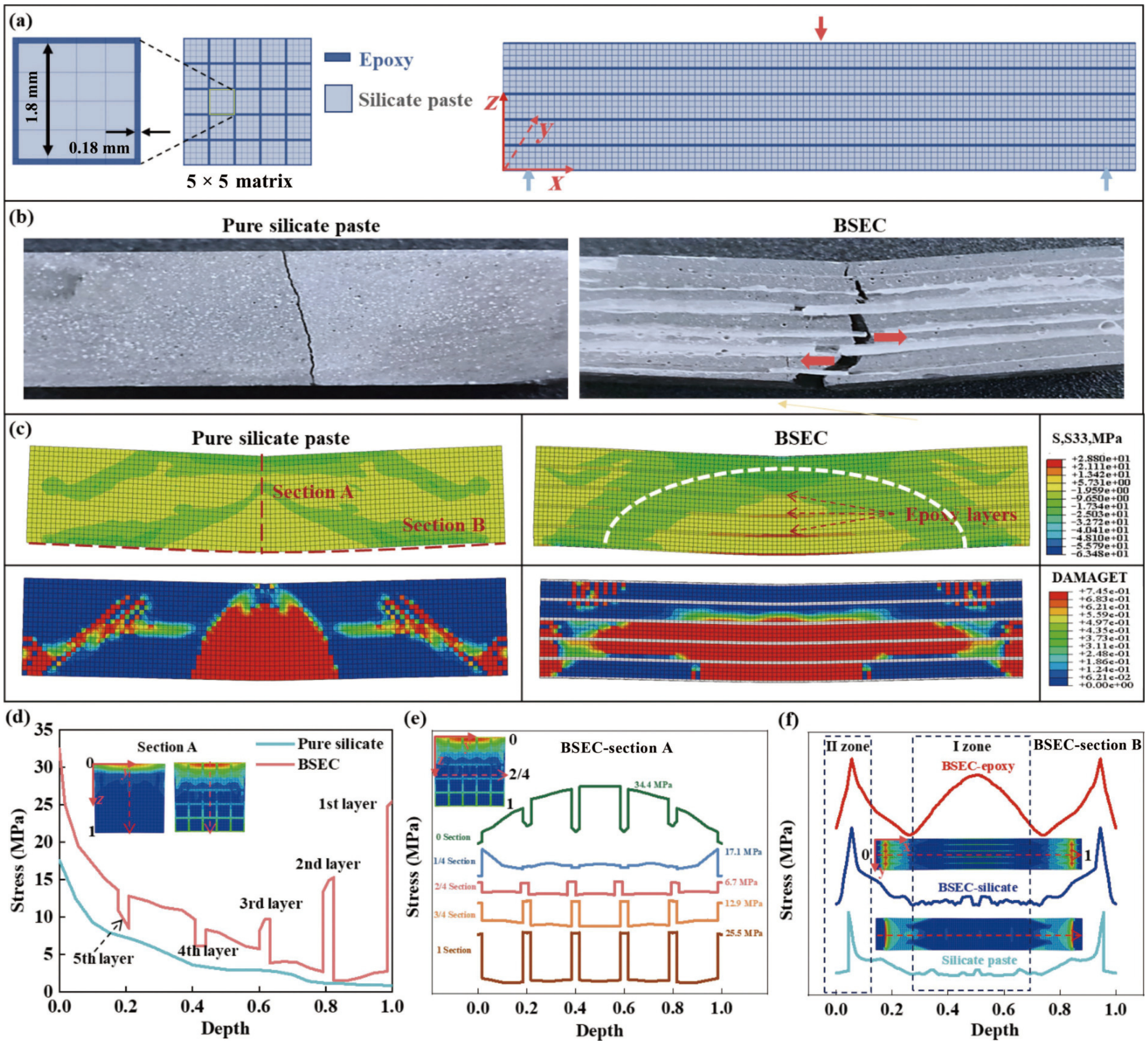

Fig. 8 Comparative investigations between numerical simulation and experimental observation of flexural deformation: (a) finite element model of biomimetic structure; (b) flexural fractural morphology; (c) Mises stress and tensile damage features; (d, e) stress variation on longitudinal section A along *z*-axis and *y*-axis, respectively; (f) stress variation of silicate and epoxy resin in cross section B.

printed biomimetic silicate-epoxy resin ceramic composites demonstrated much higher mechanical properties including compressive strength (48.8±3.12 MPa), flexural strength (10.39±1.23 MPa), and flexural toughness (218.7±54.6 kJ/m^3) than those of traditional pure silicate-based ceramic composites. In addition, the macroscopic fracture observation and FEM simulation cooperatively verifies that the elastic epoxy resin sheath network effectively inhibited crack propagation and optimized stress distribution, which made silicate-based ceramic composites with exceptionally high strength and toughness. The coaxial 3D printing method has, therefore, demonstrated its promising potential to be implemented for the tailored mechanical properties of engineering materials with specifically designed biomimetic microstructures.

Acknowledgements

The authors appreciate the financial support from the Strategic Priority Research Program of the Chinese Academy of Sciences (No. XDB 0470303), the Fund of Natural Science Foundation of China (No. 52073132), and the Fundamental Research Funds for the Central Universities (Nos. lzujbky-2022-ey02 and lzujbky-2023-eyt03).

Declaration of competing interest

The authors have no competing interests to declare that are relevant to the content of this article.

References

[1] Wegst UGK, Bai H, Saiz E, *et al.* Bioinspired structural materials. *Nat Mater* 2015, **14**: 23–36.

[2] Yang Y, Song X, Li XJ, *et al.* Recent progress in biomimetic additive manufacturing technology: From materials to functional structures. *Adv Mater* 2018, **30**: 1706539.

[3] Ni DW, Cheng Y, Zhang JP, *et al.* Advances in ultra-high temperature ceramics, composites, and coatings. *J Adv Ceram* 2022, **11**: 1–56.

[4] Wei ZY, Meng GH, Chen L, *et al.* Progress in ceramic materials and structure design toward advanced thermal barrier coatings. *J Adv Ceram* 2022, **11**: 985–1068.

[5] Li Z, Ding SQ, Yu X, *et al.* Multifunctional cementitious composites modified with nano titanium dioxide: A review. *Compos Part A Appl S* 2018, **111**: 115–137.

[6] Lawrence P, Cyr M, Ringot E. Mineral admixtures in mortars: Effect of inert materials on short-term hydration. *Cem Concr Res* 2003, **33**: 1939–1947.

[7] Birchall JD, Howard AJ, Kendall K. Flexural strength and porosity of cements. *Nature* 1981, **289**: 388–390.

[8] Li XF, Guo ZW, Huang QR, *et al.* Research and application of biomimetic modified ceramics and ceramic composites: A review. *J Am Ceram Soc* 2024, **107**: 663–697.

[9] Ritchie RO. The conflicts between strength and toughness. *Nat Mater* 2011, **10**: 817–822.

[10] Xu ZH, Li XD. Deformation strengthening of biopolymer in nacre. *Adv Funct Mater* 2011, **21**: 3883–3888.

[11] Huang YJ, Wan CL. Controllable fabrication and multifunctional applications of graphene/ceramic composites. *J Adv Ceram* 2020, **9**: 271–291.

[12] Yeom B, Sain T, Lacevic N, *et al.* Abiotic tooth enamel. *Nature* 2017, **543**: 95–98.

[13] Barthelat F, Tang H, Zavattieri PD, *et al.* On the mechanics of mother-of-pearl: A key feature in the material hierarchical structure. *J Mech Phys Solids* 2007, **55**: 306–337.

[14] Zhao XH, Chen XY, Yuk H, *et al.* Soft materials by design: Unconventional polymer networks give extreme properties. *Chem Rev* 2021, **121**: 4309–4372.

[15] Wegst UGK, Ashby MF. The mechanical efficiency of natural materials. *Philos Mag* 2004, **84**: 2167–2186.

[16] Yahyazadehfar M, Zhang DS, Arola D. On the importance of aging to the crack growth resistance of human enamel. *Acta Biomater* 2016, **32**: 264–274.

[17] Liu SY, Xu YZ, Liao RC, *et al.* On fracture behavior of inner enamel: A numerical study. *Appl Math Mech* 2023, **44**: 931–940.

[18] Zhao HW, Liu SJ, Wei Y, *et al.* Multiscale engineered artificial tooth enamel. *Science* 2022, **375**: 551–556.

[19] Chen Y, Zheng YZZ, Zhou Y, *et al.* Multi-layered cement-hydrogel composite with high toughness, low thermal conductivity, and self-healing capability. *Nat Commun* 2023, **14**: 3438.

[20] Pogorelov E, Tushtev K, Arnebold A, *et al.* Strong and super tough: Layered ceramic-polymer composites with bio-inspired morphology. *J Am Ceram Soc* 2018, **101**: 4732–4742.

[21] Meng YF, Zhu YB, Zhou LC, *et al.* Artificial nacre with high toughness amplification factor: Residual stress-engineering Sparks enhanced extrinsic toughening mechanisms. *Adv Mater* 2022, **34**: 2108267.

[22] Cheng MQ, Liu M, Chang LR, *et al.* Overview of structure, function and integrated utilization of marine shell. *Sci Total Environ* 2023, **870**: 161950.

[23] Song F, Soh AK, Bai YL. Structural and mechanical properties of the organic matrix layers of nacre. *Biomaterials* 2003, **24**: 3623–3631.

[24] Munch E, Launey ME, Alsem DH, *et al.* Tough, bio-inspired hybrid materials. *Science* 2008, **322**: 1516–1520.

[25] Chaudhary RP, Parameswaran C, Idrees M, *et al.* Additive manufacturing of polymer-derived ceramics: Materials, technologies, properties and potential applications. *Prog Mater Sci* 2022, **128**: 100969.

[26] Clegg WJ, Kendall K, Alford NM, *et al.* A simple way to make tough ceramics. *Nature* 1990, **347**: 455–457.

[27] Wang CA, Huang Y, Zan QF, *et al.* Control of composition and structure in laminated silicon nitride/boron nitride composites. *J Am Ceram Soc* 2002, **85**: 2457–2461.

[28] Chen K, Tang XK, Jia BB, *et al.* Graphene oxide bulk material reinforced by heterophase platelets with multiscale interface crosslinking. *Nat Mater* 2022, **21**: 1121–1129.

[29] Picot OT, Rocha VG, Ferraro C, *et al.* Using graphene networks to build bioinspired self-monitoring ceramics. *Nat Commun* 2017, **8**: 14425.

[30] Zhang XQ, Zhang KQ, Zhang B, *et al.* Mechanical properties of additively-manufactured cellular ceramic structures: A comprehensive study. *J Adv Ceram* 2022, **11**: 1918–1931.

[31] Dadkhah M, Tulliani JM, Saboori A, *et al.* Additive manufacturing of ceramics: Advances, challenges, and outlook. *J Eur Ceram Soc* 2023, **43**: 6635–6664.

[32] Genet M, Houmard M, Eslava S, *et al.* A two-scale Weibull approach to the failure of porous ceramic structures made by robocasting: Possibilities and limits. *J Eur Ceram Soc* 2013, **33**: 679–688.

[33] Murr LE, Gaytan SM, Ceylan A, *et al.* Characterization of titanium aluminide alloy components fabricated by additive manufacturing using electron beam melting. *Acta Mater* 2010, **58**: 1887–1894.

[34] Ortiz-Álvarez N, Lizarazo-Marriaga J, Brandão PFB, *et al.* Rheological properties of cement-based materials using a biopolymer viscosity modifying admixture (BVMA) under different dispersion conditions. *Cem Concr Compos* 2021, **124**: 104224.

[35] Stynoski P, Mondal P, Marsh C. Effects of silica additives on fracture properties of carbon nanotube and carbon fiber reinforced Portland cement mortar. *Cem Concr Compos* 2015, **55**: 232–240.

[36] Banthia N, Sappakittipakorn M. Toughness enhancement in steel fiber reinforced concrete through fiber hybridization. *Cem Concr Res* 2007, **37**: 1366–1372.

[37] Wang R, Wang PM, Li XG. Physical and mechanical properties of styrene–butadiene rubber emulsion modified cement mortars. *Cem Concr Res* 2005, **35**: 900–906.

[38] Krystek M, Pakulski D, Patroniak V, *et al.* High-performance graphene-based cementitious composites. *Adv Sci* 2019, **6**: 1801195.

[39] Dimov D, Amit I, Gorrie O, *et al.* Ultrahigh performance nanoengineered graphene–concrete composites for multifunctional applications. *Adv Funct Mater* 2018, **28**: 1705183.

[40] Liang R, Liu Q, Hou DS, *et al.* Flexural strength enhancement of cement paste through monomer incorporation and *in situ* bond formation. *Cem Concr Res* 2022, **152**: 106675.

[41] Sun GX, Liang R, Zhang JR, *et al.* Mechanism of cement paste reinforced by ultra-high molecular weight polyethylene powder and thermotropic liquid crystalline copolyester fiber with enhanced mechanical properties. *Cem Concr Compos* 2017, **78**: 57–62.

[42] Pan H, She W, Zuo WQ, *et al.* Hierarchical toughening of a biomimetic bulk cement composite. *ACS Appl Mater Interfaces* 2020, **12**: 53297–53309.

[43] Li JJ, Wan CJ, Niu JG, *et al.* Investigation on flexural toughness evaluation method of steel fiber reinforced lightweight aggregate concrete. *Constr Build Mater* 2017, **131**: 449–458.

[44] Fernández-Ruiz MA, Gil-Martín LM, Carbonell-Márquez JF, *et al.* Epoxy resin and ground tyre rubber replacement for cement in concrete: Compressive behaviour and durability properties. *Constr Build Mater* 2018, **173**: 49–57.

[45] Studart AR. Towards high-performance bioinspired composites. *Adv Mater* 2012, **24**: 5024–5044.

[46] He ZM, Shen AQ, Guo YC, *et al.* Cement-based materials modified with superabsorbent polymers: A review. *Constr Build Mater* 2019, **225**: 569–590.

[47] Fratzl P, Gupta HS , Fischer FD, *et al.* Hindered crack propagation in materials with periodically varying Young's modulus—Lessons from biological materials. *Adv Mater* 2007, **19**: 2657–2661.

[48] Barthelat F. Designing nacre-like materials for simultaneous stiffness, strength and toughness: Optimum materials, composition, microstructure and size. *J Mech Phys Solids* 2014, **73**: 22–37.